ELSEVIER

Journal of Hazardous Materials 43 (1995) 169–193

JOURNAL OF HAZARDOUS MATERIALS

Unsteady heat-transfer effects on the spreading and dilution of dense cold clouds

J.P. Kunsch*, T.K. Fanneløp

Department of Mechanical Engineering, Swiss Federal Institute of Technology, CH-8092 Zurich, Switzerland

Received 29 January 1994; accepted in revised form 21 March 1995

Abstract

The transient heating effects on cold clouds spreading, in the absence of wind, over much warmer ground surfaces, are examined. The heat flux from the ground to the cloud affects both the rate of spreading and the cloud longevity. The effects are most pronounced for surfaces that are good conductors, but substantial corrections are found for cryogenic releases on all surfaces of practical interest.

The theoretical results are applicable also to hot-fire plumes spreading under a cold ceiling. They have been verified by comparison with existing experiments in channels, i.e. a heavy-gas (cryogenic) ground release as well as a hot-fire plume under the ceiling. A simple analytic solution is also given, which shows explicitly the role of various (dimensionless) parameters. This simplified solution shows good agreement with both the exact numerical solution and the experiments and it requires only algebraic evaluation.

Keywords: Cold dense cloud; Hot plume; Unsteady heat transfer; Box model; Hazardous range

1. Introduction

Early interest in the hazards of heavy-gas releases were often related to cold clouds from cryogenic sources e.g. in connection with large-scale importation of cryogenic gases (LNG) for energy purposes. Some of the heat-transfer problems associated with accidental cryogenic releases [1], were really never solved as cheap oil became abundant later on and the research interest shifted to chemical releases at or near atmospheric temperatures.

In some early studies of cold clouds, the heat transfer analyses were based on forced convection boundary-layer concepts where the motion of the cloud relative to the ground and the specified (constant) ground temperature decided the outcome, as discussed by Raj [2]. The method results in gross under-estimation of the effects of

* Corresponding author.

SSDI 0304-3894(95)00036-4

heat transfer from the ground in comparison with that from entrainment, for low wind speeds. Colenbrander and Puttock [3] were the first to show experimentally that free convection is the dominant heat-transfer mechanism, a view confirmed by later experiments [4–6].

A sudden release of cold gas in the atmospheric boundary layer gives rise to an unsteady flow problem. For constant wind speed and after sufficient time, a maintained source produces a steady ground plume which can be simulated in a wind tunnel. The simulation requirements for cold gases are discussed by many authors, perhaps most thoroughly by Britter [7]. He concluded that natural convection is more important than forced convection for low wind speeds and smooth surfaces. It is unfortunate that free-convection effects, important both for heating and for contributing to entrainment, cannot be simulated correctly in wind tunnels. In the present paper, it will be demonstrated that the change in surface temperature, resulting from the sudden contact with the cold cloud, is an equally important effect for instantaneous releases. For LNG-clouds, in particular, the hazardous range will be limited by heat-transfer rather than entrainment effects for certain surfaces on which the cloud spreads in the absence of wind. The effects of coupling between cloud motion and heat transferred from the ground through the surface of contact, can be studied only from unsteady simulations or from time-dependent flow analysis. Such analyses have been published in the past for boiling and spreading cryogenic pools [8, 9] but not for cold clouds.

The importance of the effects considered herein depends on the thermal properties of the supporting (solid) surface. As the cold cloud front moves over a new surface area, the ground temperature is high and the contact surface subtending the cloud front is suddenly exposed to a very high rate of heat-transfer (thermal shock). This results in selective heating of the cloud frontal region, as seen from the experimental results in Zumsteg's Dissertation [10] (Fig. 1). The rate of decay of the heat-transfer rate from the initial peak value, is most pronounced for an insulating surface. All surfaces of practical interest, also good insulators, have heat capacities orders of magnitude higher than that of the gas in the cloud. It follows that the temperature rise in the cloud will be substantial also for very small thermal penetration thicknesses.

The selective heating of the front is important also for the cloud dynamics. The cloud motion is generally analysed based on a specified intrusion-velocity relation which depends on the density difference, cloud to ambient, at the front. As the loss of negative buoyancy is most pronounced in the front region, due to selective heating, cold clouds appear to be annihilated near the front and replenished from the rear where the heating effects are less severe. Although the negative buoyancy is lost, the vorticity associated with the front vortex remains, and one can sometimes observe a detached front of near ambient temperature running ahead of the cold cloud which redevelops behind [11]. The annihilation of the front due to selective heating also affects the longevity and the hazardous range of the cloud, in particular for LNG (methane) releases where neutral buoyancy occurs at temperatures well below ambient.

For a steady leak in the atmospheric wind, the final plume will be established only after considerable time which depends on the thermal properties of the ground. The

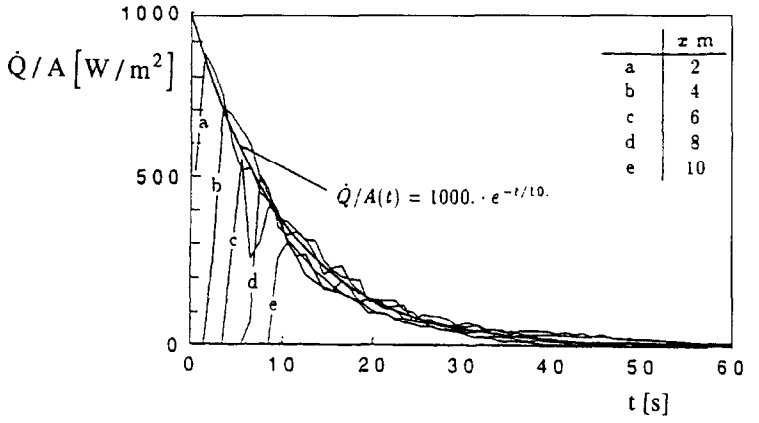

Fig. 1. Heat flux vs. time for instantaneous releases [10]. Response of heat sensor embedded in the ground surface.

initial cloud will presumably be of lesser extent due to the initially high heating rates, so that the steady-state "asymptotic" result appears to be conservative. It will be necessary, however, to consider carefully the specified front-velocity relation. The usual isothermal intrusion formula, valid for constant density (box) models, is not likely to be valid.

The spreading of cold clouds on water represents a special case as condensation and freezing of water vapour give a non-negligible contribution to the energy balance [6]. This effect will be most important for small releases with cloud height not much greater than the vapour concentration boundary layer. The Gadila experiments [12] show both strong convection currents in the gas cloud and a plume smaller than that predicted based on a steady analysis. A complete analysis of this case will not be easy. The extensive visual information available shows many interesting phenomena, but relevant measurements required for a complete analysis are not available from this field experiment. Data useful in establishing a new model exist only for the one-dimensional (planar) case, notably the cold-gas experiments of Zumsteg [10] and the hot-gas experiments of Chobotov et al. [13]. Windtunnel experiments with cryogenic gases [14] provide only the steady-state asymptotic values for reasons given.

A detailed and accurate analysis of even the simplest cloud geometry (channel flow) requires consideration of the spatial variation as well as the time dependence. The rapid variations in heat-transfer in the direction of spreading, can be accounted for in a shallow-layer model [15], whereas the observed frontal phenomena cannot. The measured heat-transfer rates indicate that a kind of similarity exists. The peak heating rates measured, as the front passes over various fixed positions x, decay at an exponential rate which depends on time only (Fig. 1). Another useful observation in formulating the analysis is that the thermal layer in the supporting surface has boundary-layer character, i.e. the conduction in the direction of spreading is negligible.

The present analysis is formulated in non-dimensional variables and it should be valid irrespective of surface and gas properties as long as the non-dimensional parameters (e.g. Stanton number) remain approximately constant. Substantial differences in the results relative to existing analytic models will be found also when a cold gas spreads on an insulating surface, such as light snow or a surface with a trapped gaseous layer (grass or gravel). Results are presented for both extremes, i.e. when a good insulator (a building material) or a good conductor (metal) are used as surface on which the cloud spreads. In addition to the case of heavy-gas dispersion, the model is of interest also for the spreading of light (hot) gases under the ceiling, a case of considerable importance in fire research. (The effects of air movement due to ventilation are not considered.)

Two methods of solving the equations describing the model are given; a numerical method based on the full equations and an iterative solution carried out to second order where the basic (first-order) solution corresponds to the case of constant cloud temperature. Good agreement is obtained between the numerically exact and the approximate solutions. The iteration solution has the practical advantage that additional numerical integrations of the differential equations are not required in applications. It displays clearly also the physical effects and the relative importance of the many parameters considered.

2. Box model including unsteady heat transfer

2.1. Basic equations

The equations are formulated with the usual box-model assumptions, for which spatial variations in the dependent variables are neglected. The density and temperature of the spreading cloud are supposed to be dependent only on time. The assumption of constant velocity and temperature over the height (tophat profiles) can be justified for a free convection layer as the strong mixing smooths all gradients [10, 15]. The assumption of spatial invariance in the direction of spreading has been shown, by comparison with the results of shallow-layer calculations [15], to be quite accurate except in a short time interval after release. The initial temperature of the surface on which the cloud spreads is assumed to be equal to the ambient temperature. A cross-section of an idealized cloud, of length X_F and height h, with temperature profiles as discussed above, is shown in Fig. 2. The equation of energy conservation in the cloud can be expressed in the 2-D case, e.g. for a channel of width B:

$$mc_p\frac{dT_c}{dt} = \rho_s\dot{V}_s c_{ps}(T_s - T_c) + \rho_a\dot{V}_a c_{pa}(T_a - T_c) + \alpha(T_w - T_c)BX_F \tag{1}$$

Three different heat fluxes on the RHS contribute to the variation in time of the temperature T_c of the cloud of mass $m(t)$.

The first term on the RHS represents a continuous source of temperature T_s and density ρ_s, with volume flow rate $\dot{V}_s$, the second term the entrainment of ambient air

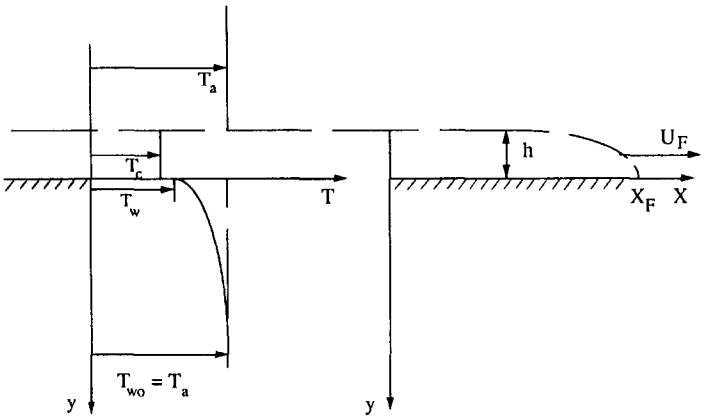

Fig. 2. Idealized temperature profiles in the cloud and the surface on which the cloud spreads.

with a volume flow rate $\dot{V}_a$ of density ρ_a and temperature T_a. The third term is related to the convective heat transfer from the ground of surface temperature T_w with heat transfer coefficient α. In the case of a sudden finite-volume release, $\dot{V}_s = 0$. This equation is discussed e.g. by Riou [16].

The problem of unsteady heat conduction in the surface on which the cloud spreads, is governed by the one-dimensional Fourier equation and has boundary-layer character. It can be solved approximately by a Pohlhausen method. To this end the Fourier equation is used in integral form with suitable profile assumptions (Fig. 2):

$$\int_0^{\delta} \frac{\partial T}{\partial t} dy = \int_0^{\delta} a \frac{\partial^2 T}{\partial y^2} dy$$

with the thermal diffusivity a and the penetration depth of the temperature perturbation δ.

On substituting the profile

$$\left(\frac{T}{T_a} - 1\right) = \left(\frac{T_w}{T_a} - 1\right)(1 - \eta)^3$$

where $\eta = y/\delta$, one obtains an ordinary differential equation where the dependence on the variable normal to the surface, on which the cloud spreads, is eliminated:

$$\frac{d}{dt}[\delta(T_w - T_a)] = 12a\frac{T_w - T_a}{\delta}. \tag{2}$$

In the case of a suddenly applied constant surface temperature T_w, the exact solution is known, i.e. $\delta = c_\delta(at)^{1/2}$. The coefficient c_δ as obtained by the approximate method differs by less than 10% from the exact value.

At the surface of contact the heat flux due to heat transfer must equal the heat flux by conduction:

$$\lambda_w \left.\frac{\partial T}{\partial y}\right|_{y=0} = \alpha(T_w - T_c)$$

with the thermal conductivity of the solid λ_w and the heat-transfer coefficient α.

This coupling condition can be written in terms of the assumed similarity profile as

$$T_w - T_a = -\frac{\alpha\delta}{3\lambda_w}(T_w - T_c). \tag{3}$$

This relates $T_w(t)$, $T_c(t)$ and $\delta(t)$.

The air entrainment at the free surface is responsible for the dilution of the cloud as expressed by the change in mass concentration c. We define $c = m_s/m$ in terms of the total mass $m = m_s + m_a$, the initial undiluted gas mass $m_s = \rho_s V_s$ and the mass of the entrained air m_a.

By differentiating the concentration c w.r.t. t, we obtain the identity:

$$\frac{dc}{dt} = c\frac{\dot{m}_s}{m_s} - c^2\frac{\dot{m}}{m_s} \tag{4}$$

with $\dot{m} = \dot{m}_s + \dot{m}_a$. In case of a sudden fixed-volume release $\dot{m}_s = \rho_s \dot{V}_s$ vanishes. The mass-flow rate of entrained air $\dot{m}_a$ is provided by means of an entrainment velocity v_e, i.e. $\dot{m}_a = \rho_a v_e B X_F$. v_e will be specified later in Section 2.3.

The total mass is

$$m = \rho h B X_F, \tag{5}$$

The equation of state for ideal gas mixtures provides the density ρ:

$$\frac{\rho}{\rho_a} = \frac{R_a T_a}{R T_c} \tag{6}$$

where $R = cR_s + (1 - c)R_a$ is the gas constant per unit mass of mixture.

The set of equations is completed by a relation for the frontal velocity that controls the dynamic behaviour of the cloud:

$$U_F = \frac{dX_F}{dt} = \left(kg\frac{\rho - \rho_a}{\rho_a}h\right)^{1/2} = \left(k\frac{\rho}{\rho_a}\right)^{1/2} C_F. \tag{7}$$

This is the familiar gravity–current relation, normally used in the formulation of the box model when constant temperature and negligible changes in density are assumed [17]. As indicated in (7), U_F is related to the propagation velocity C_F of gravity waves in the cloud. This is a "global" quantity not dependent on the local difference in density at the front.

The variation in time of the quantities T_c, T_w, δ, c, m, ρ, X_F is obtained from Eqs. (1)–(7). The ambient temperature T_a and density ρ_a, as well as the volume flow rate $\dot{V}_s$ can be considered as given boundary conditions.

The equations derived are applicable to sudden fixed-volume releases as well as to continuous constant releases with $V_s = \dot{V}_s t$. It is implied that the flow is planar, as in the investigations of Zumsteg [10] and Chobotov et al. [13]. A representation with volume and flow rate given per unit width ($Q_s = V_s/B$, $\dot{Q}_s = \dot{V}_s/B$) is normally used for this 2-D case.

2.2. Dimensionless equations

Suitable scaling variables are needed for a non-dimensional representation of the equations. In the case of an instantaneous fixed-volume release, the initial height of the volume released will be an appropriate reference length: $L_{ref} = h(t = 0)$. No geometrical dimension can be taken as a physically relevant length in the case of a continuous (point) release, but a suitable reference length can be obtained from the flow rate of the source; i.e.

$$L_{ref} = (\dot{Q}_s^2/g)^{1/3}.$$

A suitable reference speed C_{ref} will be the wave propagation velocity corresponding to the fictitious layer height: $C_{ref} = (gL_{ref})^{1/2}$, and the corresponding reference time $t_{ref} = L_{ref}/C_{ref}$. The reference temperature T_{ref} is set equal to the ambient temperature T_a. With the use of these scaling variables, a dimensionless form of the equations above can be obtained. The dimensionless groupings, which can be identified, are listed below (expressions (13a)–(13e)). Eqs. (2) and (3) yield:

$$\frac{d}{d\bar{t}}[\bar{\delta}(\bar{T}_w - 1)] = 12Fo\frac{\bar{T}_w - 1}{\bar{\delta}},$$

$$\bar{T}_w - 1 = -\tfrac{1}{3}Bi\,\bar{\delta}(\bar{T}_w - \bar{T}_c).$$

These equations are rewritten to obtain the time rate of change for the penetration depth and the cloud temperature, respectively:

$$\frac{d}{d\bar{t}}(\bar{\delta}^2) = \frac{1+\Omega}{2+\Omega}\left[24Fo - 2\bar{\delta}^2\frac{1}{\bar{T}_c - 1}\frac{d\bar{T}_c}{dt}\right] \quad \text{with} \quad \Omega(\bar{t}) = \tfrac{1}{3}Bi\bar{\delta}(\bar{t}), \tag{8}$$

$$\frac{d\bar{T}_c}{d\bar{t}} = c\frac{\dot{\bar{Q}}_s}{\bar{Q}_s}\frac{c_{ps}}{c_p}(\bar{T}_s - \bar{T}_c) - c\frac{\bar{X}_F}{\bar{Q}_s}\frac{c_{ps}}{c_p}\left[\left(\frac{\rho_a}{\rho_s}\right)\left(\frac{c_{pa}}{c_{ps}}\right)\bar{v}_e(\bar{T}_c - 1) - St(\bar{T}_w - \bar{T}_c)\right]. \tag{9}$$

The temperature of the surface of contact is given by the non-dimensional form of Eq. (3):

$$\bar{T}_w - 1 = \frac{\Omega}{1+\Omega}(\bar{T}_c - 1). \tag{10}$$

The rate of change with time of the concentration is found from (4) to be

$$\frac{dc}{d\bar{t}} = c(1-c)\frac{\dot{\bar{Q}}_s}{\bar{Q}_s} - c^2\frac{\bar{X}_F}{\bar{Q}_s}\left(\frac{\rho_a}{\rho_s}\right)\bar{v}_e. \tag{11}$$

The position of the front, in accord with (6) and (7), is

$$\frac{\mathrm{d}}{\mathrm{d}\bar{t}}(\bar{X}_{\mathrm{F}}^{3/2}) = \frac{3}{2}Fr\left[\left|1 - \frac{\rho_{\mathrm{a}}}{\rho}\right|\frac{1}{c}\bar{Q}_{\mathrm{s}}\right]^{1/2} \quad \text{with} \quad \frac{\rho_{\mathrm{a}}}{\rho} = \left[(1-c) + c\left(\frac{R_{\mathrm{s}}}{R_{\mathrm{a}}}\right)\right]\bar{T}_{\mathrm{c}}. \tag{12}$$

The relevant dimensionless groupings are summarized as follows:

$$\text{Froude number:} \quad Fr = \frac{U_{\mathrm{F}}}{C_{\mathrm{F}}} = (k\,\rho_{\mathrm{s}}/\rho_{\mathrm{a}})^{1/2}, \tag{13a}$$

$$\text{Stanton number:} \quad St = \alpha/\rho_{\mathrm{s}}c_{\mathrm{ps}}C_{\mathrm{ref}}, \tag{13b}$$

$$\text{Fourier number:} \quad Fo = \frac{at_{\mathrm{ref}}}{L_{\mathrm{ref}}^2}, \tag{13c}$$

$$\text{Biot number:} \quad Bi = \frac{\alpha L_{\mathrm{ref}}}{\lambda_{\mathrm{w}}}, \tag{13d}$$

$$\text{Dimensionless entrainment:} \quad \bar{v}_{\mathrm{e}} = \frac{v_{\mathrm{e}}}{C_{\mathrm{ref}}}. \tag{13e}$$

In the case of an instantaneous fixed-volume release, the non-dimensional volume of gas is expressed as

$$\bar{Q}_{\mathrm{s}} = \frac{Q_{\mathrm{s}}}{L_{\mathrm{ref}}^2}$$

and in the case of a continuous source release as

$$\bar{Q}_{\mathrm{s}} = \bar{q}_{\mathrm{s}}\bar{t} \quad \text{with} \quad \bar{q}_{\mathrm{s}} = \dot{Q}_{\mathrm{s}}/(gL_{\mathrm{ref}}^3)^{1/2}. \tag{13f}$$

The remaining dimensionless groupings occurring in the equations are the density ratio, the ratio of specific heats and the ratio of the relevant gas constants:

$$\left(\frac{\rho_{\mathrm{s}}}{\rho_{\mathrm{a}}}\right), \left(\frac{c_{\mathrm{pa}}}{c_{\mathrm{ps}}}\right) \quad \text{and} \quad \left(\frac{R_{\mathrm{a}}}{R_{\mathrm{s}}}\right), \tag{13g}$$

where for ideal gases $(R_{\mathrm{a}}/R_{\mathrm{s}})$ could be replaced by $(T_{\mathrm{a}}/T_{\mathrm{s}})$ etc.

These groupings have been identified also by Britter [7] who discussed the modelling requirements for similarity between model experiments and full scale. In addition to equal Froude number, Stanton number, etc. full similarity requires that the scaled volumes (13f) and the ratios (13g) are equal in model and full scale. The last conditions are important when the gases in the initial cloud have thermodynamic properties different from that of air. The thermodynamic state in the spreading cloud will depend both on molecular properties and on the temperature difference relative to the entrained air.

The physical importance of the remaining similarity parameters is well known. The Stanton number models the surface heat transfer. The Fourier number characterizes

the properties of the surface on which the cloud spreads and compares the characteristic length L_{ref} with an approximate penetration depth in a given time t_{ref} of a change in surface temperature. The Biot number describes the coupling between the surface on which the cloud spreads and the cloud. It compares internal-conduction resistance with surface-convection resistance. A very low value of the Biot number implies that the temperature will be nearly uniform throughout the surface on which the cloud spreads. The dimensionless entrainment velocity $\bar{v}_e$ models the entrainment of ambient air by the spreading cloud. The Froude number Fr compares the frontal velocity U_F with the propagation velocity of gravity waves C_F. The frontal condition (13a) gives the initial Froude number, defined in terms of the density of the undiluted gas ($\rho = \rho_s$).

2.3. *Physical input to the model and basic assumptions*

The entrainment in the frontal region will be strongly influenced by the front vortex, when present. The entrainment associated with free convection will be more evenly distributed over the top surface. To the extent that the spreading velocity contributes to entrainment, it will be most pronounced near the front (high velocity) and vanish near the centre. Underlying the present model are the shallow-layer assumptions with entrainment primarily from free convection. For entrainment rates we refer to the experiments of Ruff et al. [6] who studied heavy-gas dispersion from continuous sources in a channel. Calculations with a shallow-layer code [18] show that for an entrainment velocity $v_e = 0.007$ m/s, optimal agreement with the temperature profiles and the heat flux through the floor, as measured by Zumsteg [10] for instantaneous releases, can be obtained. In Fig. 6 it is demonstrated that this average entrainment velocity is also reasonable in connection with the box model. We therefore adopt a constant, uniform entrainment rate. Its value reflects the importance of the high rates of heat transfer and differs from that applicable to isothermal flows.

The chosen frontal condition does not describe accurately the initial acceleration phase as discussed by Fanneløp [17]. Recent correlations of Froude numbers for a wide range of density ratios are provided by Gröbelbauer et al. [19] for heavy as well as for light-gas fronts in closed channels (exchange flows). Extrapolations to open channels are also presented. The Froude numbers required for specification of the frontal speed, in the case of present interest, can be extracted from these correlations. They are in good agreement with Zumstegs' observations [10] relative to cold nitrogen clouds (providing values for k in the frontal condition) and also for Chobotov et al.'s measurements of the Richardson number in a light-gas cloud emanating from a continuous source under the ceiling of a channel.

Although there is still some discussion about the exact mechanisms of heat transfer in the free convection process, empirical correlations for the Nusselt number $Nu = \alpha L_{ref}/\lambda$, with the thermal conductivity of the cloud λ, converge towards a unique expression: $Nu = c_N\, Ra^n$ with $n = \frac{1}{3}$ (see e.g. [7]). There is considerable scatter in the proposed value for the constant c_N, ranging from about 0.15 to 0.21 depending on author. Britter recommends a value of $c_N = 0.19$. It follows for the heat transfer

coefficient

$$\alpha = \frac{\lambda}{L_{\text{ref}}} Nu = c_{\text{N}} \frac{\lambda}{L_{\text{ref}}} Ra^{1/3} \quad \text{with } Ra = \frac{g\beta L_{\text{ref}}^3 \Delta T}{va}$$

valid for a cold cloud over a heated surface and a hot plume under a cold ceiling. With an exponent $n = \frac{1}{3}$ it can be shown that the heat-transfer coefficient α is independent of the characteristic geometric dimensions (see e.g. [20]). The temperature at the surface of contact and an averaged temperature of the free convection layer can be used to determine the relevant temperature difference ΔT, i.e. $\Delta T = T_{\text{w}} - T_{\text{c}}$.

Evaluation of the Ra number and the Pr number shows that no penetrative convection occurs for the cold cloud and that the flow is fully turbulent (see e.g. [21]). The constant, uniform entrainment rate, adopted in what follows, can hence be justified on this basis.

2.4. *Modes of release and integration procedure*

The rates of change of the quantities $\bar{\delta}$, $\bar{T}$, $\bar{T}_{\text{w}}$, c and $\bar{X}_{\text{F}}$ (or of their powers) are expressed explicitly by Eqs. (8)–(12). They can be integrated numerically, e.g. with the aid of a Runge–Kutta scheme, but first let us examine approximate analytic solutions. These are also important for the numerical integration in order to understand the singularities at $\bar{t} = 0$.

Two release modes are of interest: The *instantaneous fixed-volume release* is characterized by a constant volume of gas: $\bar{Q}_{\text{s}} = \bar{Q}_{\text{s}}(t = 0)$ and $\dot{\bar{Q}}_{\text{s}} = 0$. In the case of a cloud with constant temperature and constant concentration, the relation for the frontal position is (see e.g. [17]):

$$\bar{X}_{\text{F}} = \left(\frac{3}{2} Fr\right)^{2/3} \left(\frac{\rho_{\text{s}} - \rho_{\text{a}}}{\rho_{\text{s}}} \bar{Q}_{\text{s}}\right)^{1/3} \bar{t}'^{2/3} = c_0 \bar{t}'^{2/3}. \tag{14}$$

A time shift has been introduced in order to take into account the initial position of the front:

$$\bar{t}' = \bar{t} + \bar{t}_0 = \bar{t} + [\bar{X}_{\text{F}}(t = 0)/c_0]^{3/2}.$$

A continuous source release can be described by $\bar{Q}_{\text{s}} = \bar{q}_{\text{s}} \bar{t}$ and $\dot{\bar{Q}}_{\text{s}} = \bar{q}_{\text{s}}$. When heat transfer and entrainment are neglected, the following expression for the position of the front is obtained:

$$\bar{X}_{\text{F}} = Fr^{2/3} \left(\frac{\rho_{\text{s}} - \rho_{\text{a}}}{\rho_{\text{s}}} \bar{q}_{\text{s}}\right)^{1/3} \bar{t} = c_1 \bar{t}, \tag{15}$$

where the position varies linearly with time (see [17]).

The singularities appearing in the equations at $\bar{t} = 0$ for the temperature and concentration are removed by a development in a power series in time. The rate of

change with time is then

$$\left.\frac{\mathrm{d}\bar{T}_c}{\mathrm{d}\bar{t}}\right|_{\bar{t}=0} = -\frac{1}{2}\frac{c_1}{\bar{q}_s}\left[\left(\frac{\rho_a}{\rho_s}\right)\left(\frac{c_{pa}}{c_{ps}}\right)\bar{v}_e + St\right](\bar{T}_s - 1) \tag{16a}$$

$$\left.\frac{\mathrm{d}c}{\mathrm{d}\bar{t}}\right|_{\bar{t}=0} = -\frac{1}{2}\frac{c_1}{\bar{q}_s}\left(\frac{\rho_a}{\rho_s}\right)\bar{v}_e. \tag{16b}$$

In the case of a continuous source and non-vanishing heat transfer, the proposed model is valid only for early times for reasons discussed in the following.

3. Approximate analytic solution

Approximate analytic expressions are of interest as they allow rapid estimates of the evolution of cloud variables and moreover show how the various parameters influence the spreading process and the cloud properties. The expressions relevant to (a) instantaneous, fixed-volume releases and (b) suddenly started constant sources are derived separately by means of the same iteration method.

3.1. Instantaneous fixed-volume release

In a first approximation, heat transfer and air entrainment are neglected: $\bar{T}_c = \bar{T}_s$ and $c = 1$. The front position of a cloud with constant temperature and constant concentration is given then by Eq. (14):

$$\bar{X}_{F0} = c_0 \bar{t}'^{2/3}.$$

This result is used in the expression defining the concentration:

$$c = \frac{\bar{m}_s}{\bar{m}} = \frac{\bar{m}_s}{\bar{m}_s + \bar{m}_a} \quad \text{with} \quad \dot{\bar{m}}_a = \left(\frac{\rho_a}{\rho_s}\right)\bar{v}_e \bar{X}_F \cong \left(\frac{\rho_a}{\rho_s}\right)\bar{v}_e \bar{X}_{F0}$$

to yield an improved result:

$$c = \left[1 + \frac{3}{5}\left(\frac{\rho_a}{\rho_s}\right)\bar{v}_e \frac{c_0}{\bar{Q}_s}(\bar{t}'^{5/3} - \bar{t}_0^{5/3})\right]^{-1}. \tag{17}$$

An approximation for the penetration depth, for small $\bar{\delta}$, is obtained from (8):

$$\frac{\mathrm{d}(\bar{\delta}^2)}{\mathrm{d}\bar{t}} = 12\,Fo \quad \text{with solution } \bar{\delta} = (12 Fo\, \bar{t})^{1/2}. \tag{18}$$

The rate of change with time of the temperature in the cloud is derived from (9) and (10):

$$\frac{\mathrm{d}\bar{T}_c}{\mathrm{d}\bar{t}} = -c\frac{\bar{X}_F}{\bar{Q}_s}\left(\frac{c_{ps}}{c_p}\right)\left[\left(\frac{\rho_a}{\rho_s}\right)\left(\frac{c_{pa}}{c_{ps}}\right)\bar{v}_e + \frac{St}{1+\Omega}\right](\bar{T}_c - 1) \quad \text{with } \Omega = \frac{1}{3}Bi\bar{\delta}.$$

$\bar{X}_F$ is now approximated by $\bar{X}_{F0}$ and it is assumed, moreover, that the specific heats do not differ much. The concentration is given by the improved expression (17). The equation for $\bar{T}_c$ can then be simplified:

$$\frac{d\bar{T}_c}{d\bar{t}} = -c\frac{\bar{X}_{F0}}{\bar{Q}_s}\left[\left(\frac{\rho_a}{\rho_s}\right)\bar{v}_e + \frac{St}{1+\Omega}\right](\bar{T}_c - 1).$$

To make the integration easier, Ω is rewritten as follows:

$$\Omega = \frac{1}{3}Bi\,\bar{\delta} \approx \frac{\alpha}{b}\sqrt{\bar{t}} \quad \text{with } b = \sqrt{\lambda_w \rho_w c_w} \quad \text{and} \quad \bar{t} = \bar{t}' - \bar{t}_0.$$

The coefficient b is a measure of the heat penetration and it is a characteristic of the material. In the case of good conductors with large heat capacities, b is large and therefore

$$1 + \Omega \approx 1 + \varepsilon\sqrt{\bar{t}} \quad \text{with } \varepsilon \ll 1.$$

The integration by parts of the equation for $\bar{T}_c$, when only terms of first order in ε are retained, gives

$$\bar{T}_c - 1 = (\bar{T}_s - 1)c^A \quad \text{with } A = 1 + \left(\frac{\rho_s}{\rho_a}\right)\frac{1}{\bar{v}_e}\frac{St}{(1+\Omega)}. \tag{19a,b}$$

It is shown below that this result is accurate for most common gas cloud/surface material combinations as $\varepsilon \ll 1$. In our case $\varepsilon < 0.01$ has been obtained for concrete, metals, etc. In the case of good insulators, this condition is not fulfilled and the approximate solution is not recommended.

It should be noted that the condition for small ε limits the validity of the approximate analytic solution to early times, i.e. $\bar{t} \ll 1/\varepsilon^2$. On the other hand, the approximate analytic solution agrees with the numerical results (see e.g. Fig. 4) even as Ω becomes large. The reason is that heat transfer through the floor surface occurs primarily when Ω is small, when the approximation is valid.

In case of no heat transfer by entrainment, Eq. (19a) is:

$$\bar{T}_c - 1 = (\bar{T}_s - 1)\exp\left[-\frac{3}{5}\frac{c_0}{\bar{Q}_s}\frac{St}{(1+\Omega)}(\bar{t}'^{5/3} - \bar{t}_0^{5/3})\right]. \tag{19c}$$

The calculation of the frontal position is reduced to the numerical evaluation of an integral:

$$\bar{X}_F^{3/2} = \bar{X}_F^{3/2}(t=0) + c_0^{3/2}\int_{\bar{t}_0}^{\bar{t}'}\left[\frac{(1-\rho_a/\rho)}{(1-\rho_a/\rho_s)}\frac{1}{c}\right]^{1/2} d\bar{t}' \tag{20}$$

with

$$\frac{\rho_a}{\rho} = \left[(1-c) + c\frac{R_s}{R_a}\right]\bar{T}_c.$$

The front velocity is hence

$$\bar{U}_F = \frac{d\bar{X}_F}{d\bar{t}} = Fr\left[\left|1 - \frac{\rho_a}{\rho}\right|\frac{1}{c}\frac{\bar{Q}_s}{\bar{X}_F}\right]^{1/2}. \tag{21}$$

The temperature of the surface of contact is given by Eq. (10) which is valid for all values of Ω:

$$\bar{T}_w - 1 = \frac{\Omega}{1+\Omega}(\bar{T}_c - 1). \tag{22}$$

The equation for the heat flux, restricted to small values of Ω, is

$$\dot{\bar{q}} = \frac{St}{1+\Omega}(1 - \bar{T}_s)c^A \tag{23a}$$

with the exponent A given by Eq. (19b).

In the special case of vanishing entrainment, we obtain:

$$\dot{\bar{q}} = \frac{St}{1+\Omega}(1 - \bar{T}_s)\exp\left[-\frac{3}{5}\frac{St}{(1+\Omega)}\frac{c_0}{\bar{Q}_s}(\bar{t}'^{5/3} - \bar{t}_0^{5/3})\right] \tag{23b}$$

or without the time shift $\bar{t}_0$

$$\dot{\bar{q}} = \frac{St}{1+\Omega}(1 - \bar{T}_s)\exp\left[-\frac{3}{5}\frac{St}{(1+\Omega)}\frac{\bar{X}_{F0}\bar{t}}{\bar{Q}_s}\right]. \tag{23c}$$

The approximate solutions have been evaluated for the case of a well insulated as well as a range of moderately to highly conducting surfaces. The results are shown in Figs. 3 and 4 where they are compared with the results of the numerical integrations. Good agreement is obtained for all quantities of interest. The properties of cold nitrogen are used in all calculations because the experimental results provided by Zumsteg [10] were obtained with this gas.

It is shown in the following that the cloud dynamics and longevity depend strongly on the properties of the floor as reflected by the Fourier number and the Biot number already discussed in Section 2.2. The data used to obtain the results shown in Fig. 3 correspond to the experimental conditions of Zumsteg [10] where a good insulator (Roofmate) was used for the ground surface. Fig. 4 presents results corresponding to a good conductor (aluminium). Physical insight can be gained from the analytical expression for $\bar{T}_w$, i.e. Eq. (22). It should be pointed out that no approximation has been performed in this equation, so that the conclusions for the limiting cases for small Ω or large Ω are general. In the case of a good insulator, the internal conduction resistance can exceed the surface convection resistance and the Biot number will be large. It follows that Ω increases rapidly with time and, in the limiting case, the temperature of the surface of contact will equal the temperature of the cloud. In the case of a good conductor and small Biot number, Ω would remain small and the

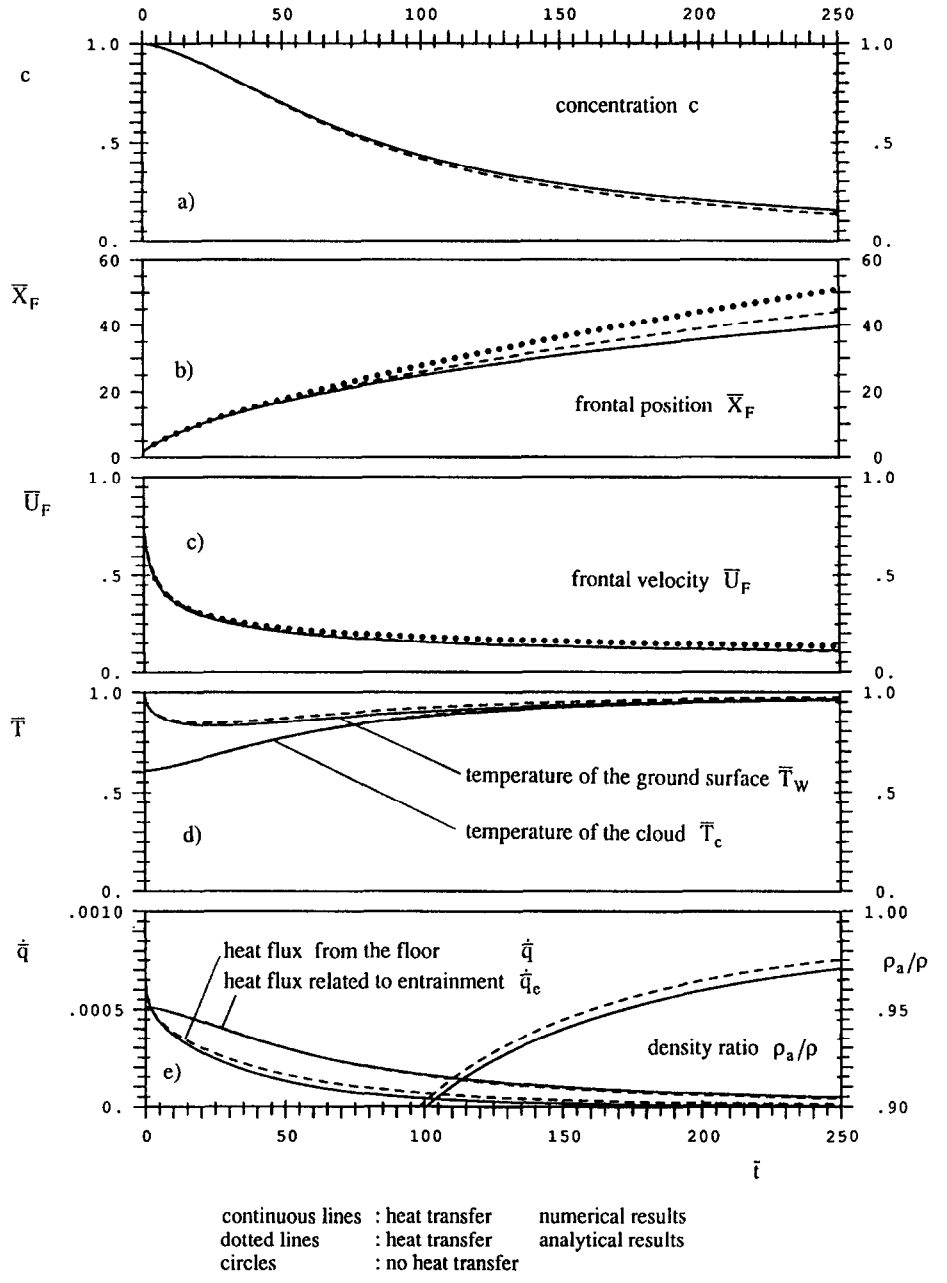

Fig. 3. Scaled time history of a cold cloud released instantaneously over a well insulated floor (nondimensional variables).

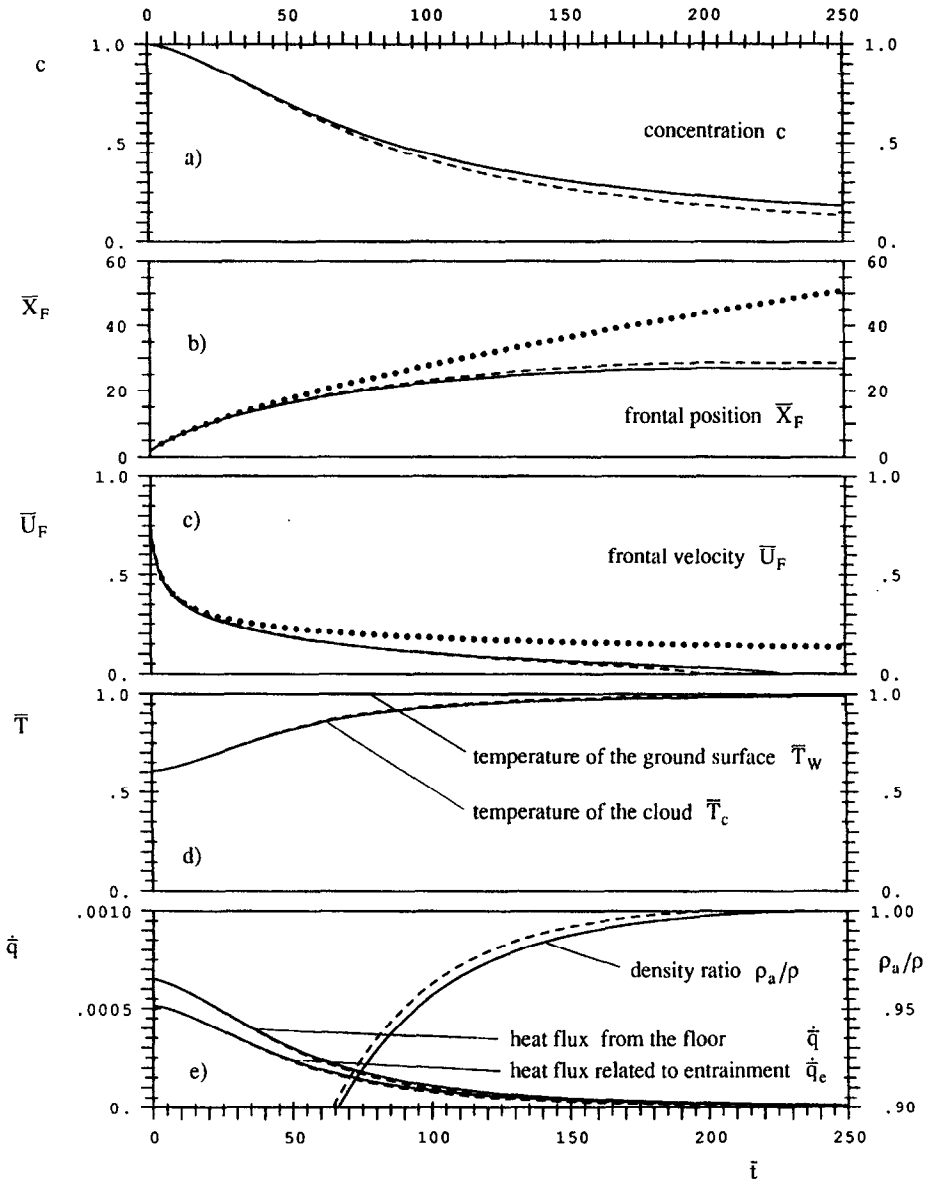

Fig. 4. Scaled time history of a cold cloud released instantaneously over a highly conducting floor (nondimensional variables).

cooling of the surface, on which the cloud spreads, would be small. The temperature profile would be near uniform and, in case it is of infinite depth, the surface would maintain a temperature close to the initial value. Should the surface be of finite (small) thickness, a uniform cooling would occur. The temperature change would be very small for materials with high heat capacities and the process could be described by a lumped-capacity model (e.g. [22]).

Eq. (23c) can be interpreted in an analogous way. It should be pointed out here, that this expression is limited to early time.The heat flux $\dot{\bar{q}}$ contributes to a loss in potential energy and the factor preceding the exponential term shows that the value of $\dot{\bar{q}}$ depends directly on the temperature difference between the source and the ambient. A large internal conduction resistance in comparison with the surface convection resistance, (i.e. large Biot number), would promote a strong increase of Ω with time and therefore a rapid decrease of $\dot{\bar{q}}$. This effect can be observed in the experiments of Zumsteg. This rapid decrease is characteristic of insulators. The exponential term in Eq. (23c) describes the change in thermal energy due to heat transfer by free convection. The temperature difference between the cloud and the surface of contact, and consequently the heat flux, is reduced as well. The heating of the cloud due to convection and the corresponding decay rate of the heat flux through the surface, are most pronounced for small release volumes. The time integral of $\bar{X}_F \dot{\bar{q}}$ is a measure of the total amount of energy transferred.

Figs. 3(e) and 4(e) present the scaled time history of the density ratio ρ_a/ρ. It approaches unity at late times (right scale). In the case the surface on which the cloud spreads is insulated (Fig. 3), the initial (averaged) temperature difference between the cloud and the surface of contact (i.e. also the heat flux) decreases rapidly. Without heat transfer, the negative buoyancy is conserved, in the absence of entrainment. It follows that the complete loss of potential energy would occur at very late times. The validity of the model would be questionable in this limit, in view of the assumptions made.

Fig. 4 illustrates the other extreme of a highly conducting surface (aluminium) where the high rate of heat transfer rapidly "kills" the cloud. This is evident by the arrested frontal position on Fig. 4(b). It is interesting to note that, at the point where its rate of progress vanishes, the cloud front has travelled only about half as far as the front of the cloud spreading on a perfect insulator. We note that the most important cryogenic gas, methane (or LNG) is lighter than air at standard conditions, so that neutral buoyancy would occur long before the cloud temperature has attained the ambient value. It must be kept in mind that in the considerations above, a condition of "no wind" has been assumed.

Closer to practical applications would be the spreading over concrete, asphalt and compact snow. The influence of these materials on the thermal behaviour of the cloud is quantitatively very similar to that of a good conductor, as revealed by time histories almost identical to those of Fig. 4, despite the considerable differences in their thermal properties. For insulating surfaces (light snow, loose gravel, dry grass, etc.) relevant thermal properties are not available. The decisive parameter is the Biot number which in our investigations ranges from 0.05 to 25 for the conducting materials mentioned, as opposed to a Biot number characterizing the coupling between the cloud and a surface made of Roofmate, i.e. $Bi = 320$.

Perhaps the most interesting result is the apparent reduction in hazardous range under no-wind conditions, in comparison with results from conventional prediction methods, for clouds from cryogenic sources spreading on conducting surfaces. It is found that common materials like concrete, asphalt, mortar and even compact snow fall in this category. The approximate analytical expressions given herein are most accurate for good conductors, but also adequate in the case of good insulators. The analytical results allow rapid estimates of the hazardous range of cold clouds with little effort.

3.2. *Continuous one-dimensional release in calm air*

The front position of a cloud with constant temperature and negligible entrainment, has already been given, i.e. Eq. (15):

$$\bar{X}_F \cong \bar{X}_{F0} = c_1 \bar{t}.$$

This result together with $\bar{Q}_s = \bar{q}_s \bar{t}$ can be used in Eq. (11) which gives the rate of change in concentration:

$$\frac{dc}{d\bar{t}} = c(1-c)\frac{1}{\bar{t}} - c^2 \frac{c_1}{\bar{q}_s}\left(\frac{\rho_a}{\rho_s}\right)\bar{v}_e. \tag{24}$$

Upon integration

$$c = \left(1 + \frac{1}{2}A\bar{t}\right)^{-1} \quad \text{where } A = \frac{c_1}{\bar{q}_s}\left(\frac{\rho_a}{\rho_s}\right)\bar{v}_e. \tag{25a, b}$$

With the assumptions discussed in the case of an instantaneous fixed-volume release, the rate of change of the temperature is given by

$$\frac{d\bar{T}_c}{d\bar{t}} = \frac{c}{\bar{t}}(\bar{T}_s - 1) - c\left\{\frac{1}{\bar{t}} + \frac{c_1}{\bar{q}_s}\left[\left(\frac{\rho_a}{\rho_s}\right)\bar{v}_e + St\right]\right\}(\bar{T}_c - 1) \tag{26}$$

with solution

$$(\bar{T}_c - 1) = (\bar{T}_s - 1)\frac{2}{A(-1 + 2B/A)}\frac{1}{\bar{t}}(1 - c^{-1+2B/A}). \tag{27a}$$

In case of no heat transfer through entrainment, the solution is

$$(\bar{T}_c - 1) = (\bar{T}_s - 1)\frac{1}{B\bar{t}}[1 - \exp(-B\bar{t})]. \tag{27b}$$

To find the frontal position, the following integral must be evaluated numerically:

$$\bar{X}_F^{3/2} = \frac{3}{2}c_1^{3/2}\int_0^{\bar{t}}\left[\frac{(1-\rho_a/\rho)}{(1-\rho_a/\rho_s)}\frac{1}{c}\bar{t}\right]^{1/2} d\bar{t} \quad \text{with} \quad \frac{\rho_a}{\rho} = \left[(1-c) + c\frac{R_s}{R_a}\right]\bar{T}_c. \tag{28}$$

A comparison of the approximate analytical results (dashed line) with numerical results (continuous line) is shown on Fig. 5. The first-order results which neglect heat-transfer effects are identified by the small black circles.

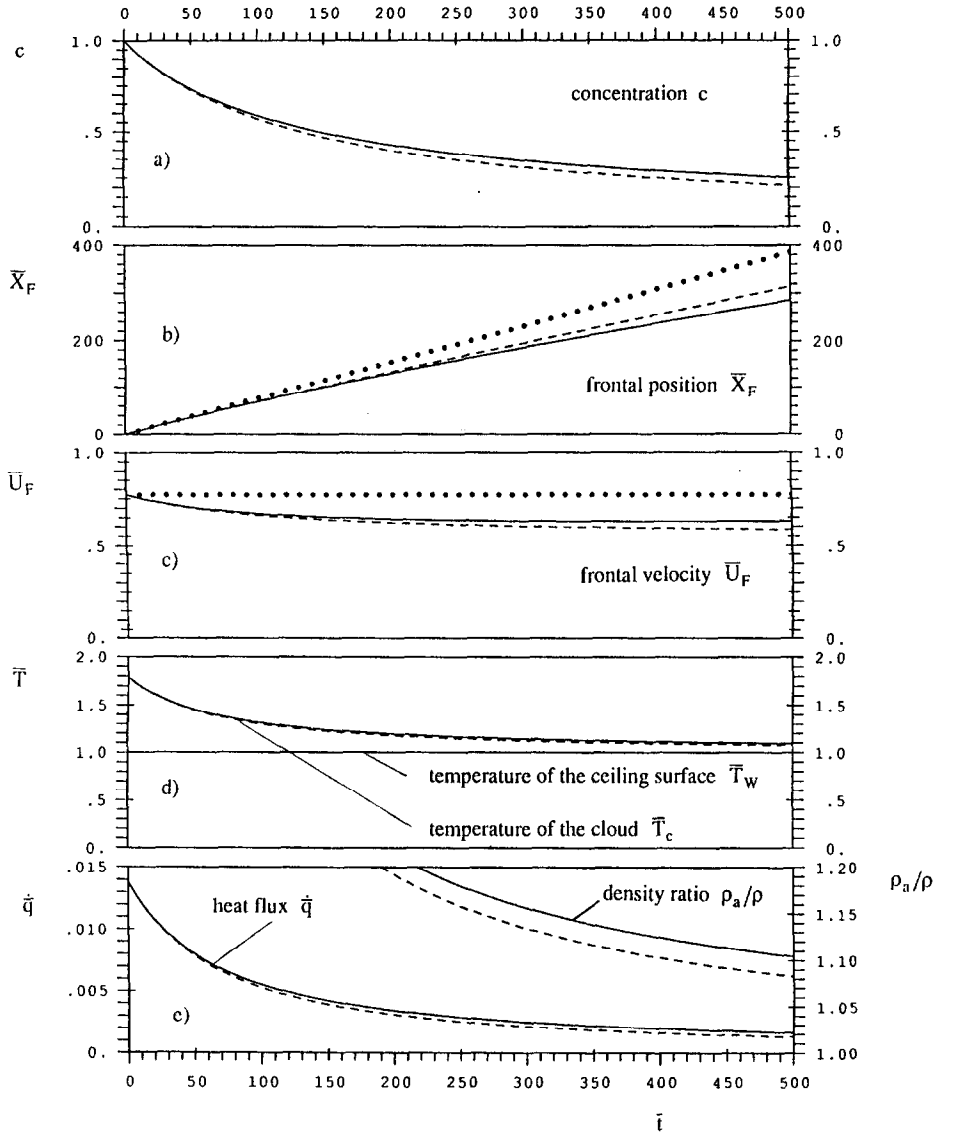

Fig. 5. Scaled time history of a heated plume from a continuous source spreading under a highly conducting ceiling (nondimensional variables).

Some consequences of the heat-transfer process, and also some limitations of the proposed model, will be demonstrated with the aid of two test cases.

4. Verification of the method and discussion

4.1. Cold cloud

The first case is concerned with the sudden release of cold (liquefied) nitrogen evaporated on water [10]. Despite the observed stratification in the source region, where evaporation takes place (the so-called starting element), the properties of the initial volume are assumed here to be homogeneous. Temperature measurements at floor level and at various locations above the floor are available at a distance of about 0.2 m from the source. The temperatures in the ground surface were recorded at different locations from the starting element.

The characteristic data of the release under consideration are: $\rho_a = 1.20\ \mathrm{kg/m^3}$, $\rho_s = 1.87\ \mathrm{kg/m^3}$. The geometric dimensions of the initial volume are: height $h_0 = 1.09$ m and length $\bar{X}_F(t = 0) = 1.82$ m. The ground surface consisted of a commercial insulating material (Roofmate) with properties: $\lambda_w = 0.036\ \mathrm{W/m\,K}$; $\rho_w = 30\ \mathrm{kg/m^3}$ and $c_w = 1300\ \mathrm{J/kg\,K}$. With these data the densimetric Froude number of the front is close to unity according to the correlations of Gröbelbauer et al. [19] and in agreement with the measurements of Zumsteg [10].

According to published correlations for the Nusselt number (see e.g. [22]), the coefficient of heat transfer depends on quantities such as the temperature of the film and the temperature difference between the cloud and the floor, quantities which vary with time. When the source conditions instead of the time-dependent conditions are used to estimate the thermal diffusivity α, consistent values are obtained for all quantities of interest (see e.g. [18]).

It can be shown furthermore that corresponding estimates, assuming heat transfer by forced convection, would show a much smaller effect in disagreement with experimental observations (see [10]).

Calculations for $\bar{T}_c$, $\bar{T}_w$ and $\dot{\bar{q}}$ are shown in Fig. 6. They compare favourably with the experimental values. Despite the well insulated floor surface, heat transfer cannot be neglected. The rapid cooling of the upper surface layer and the corresponding decay of $\dot{\bar{q}}$ are characteristic for insulating materials as seen explicitly in the (approximate) analytical solution. It can be seen also that the entrained air contributes both to the heating of the cloud, and to a reduction of the temperature difference between the cloud and the floor surface and thus of the corresponding heat flux.

4.2. Hot plume

The second case used for verification deals with a continuous source of heated nitrogen [13]. The plume under consideration spreads under the ceiling of a channel with quadratic cross section and height 0.5 m. Two cases are considered. The flow characteristics for the first case (strongly heated source) are $\rho_s = 0.628\ \mathrm{kg/m^3}$

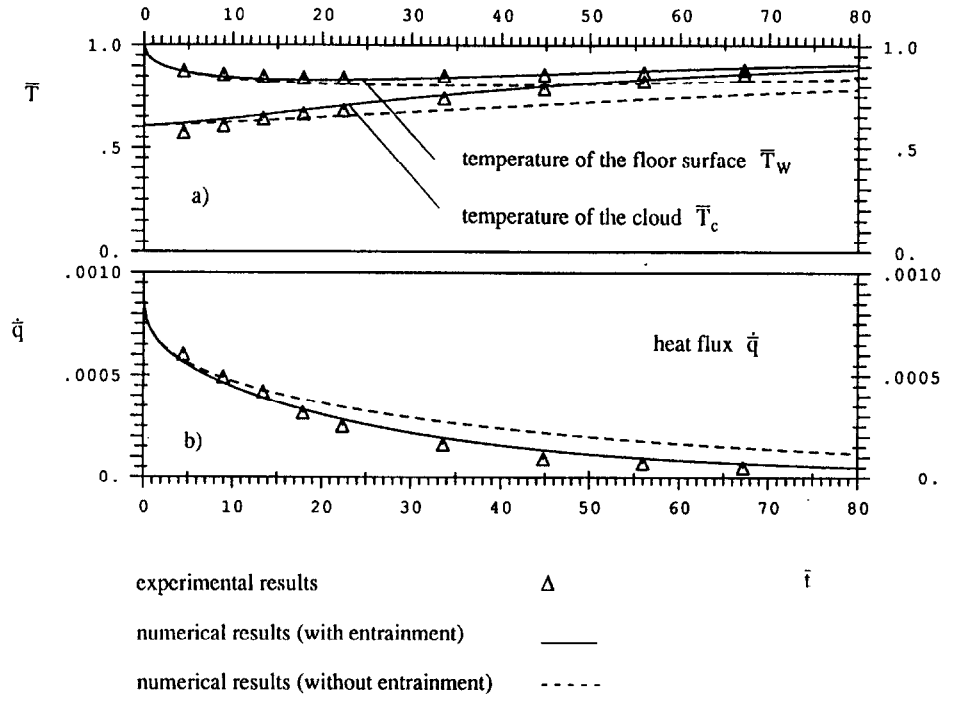

Fig. 6. Comparison of theoretical results with experiments [10] for a cold cloud released instantaneously.

($T_s = 536$ K) and $\dot{V}_s = 0.015$ m^3/s and for the second (slightly heated source) $\rho_s = 1.045$ kg/m^3 ($T_s = 322$ K) and $\dot{V}_s = 0.009$ m^3/s. In the experiments the ceiling consisted of an aluminium plate of 0.0125 m thickness. The density of the ambient air was 1.16 kg/m^3. The front behaved like an intrusion as about 15% to 20% of the channel cross section was occupied by the heated layer. The corresponding densimetric Froude number is about unity, for this layer-to-channel depth ratio, from the correlations presented by Gröbelbauer et al. [19] and this value is confirmed by the Richardson numbers given by Chobotov et al. [13] evaluated for the whole length of the plume. The Richardson number is defined in terms of the heated layer thickness h, the density parameter $\Delta = (\rho_a - \rho)/\rho_a$ and the maximum of the local velocity profile U_{Max}, i.e. $Ri = \Delta g h/U_{Max}^2$. For lack of detailed information, a constant entrainment velocity $v_e = 0.007$ m/s has been adopted, i.e. the same value as for the cold cloud. This can be justified as both cases represent free convection flows in the fully turbulent regime. The present case is dominated by heat transfer from the ceiling and the results are not sensitive to small changes in v_e.

The theoretical calculations are compared with the experimental results in Fig. 7. In the case of the slightly heated plume, it is evident that heat transfer is not important. At the end of the range of observation, the front position differs from that of a plume

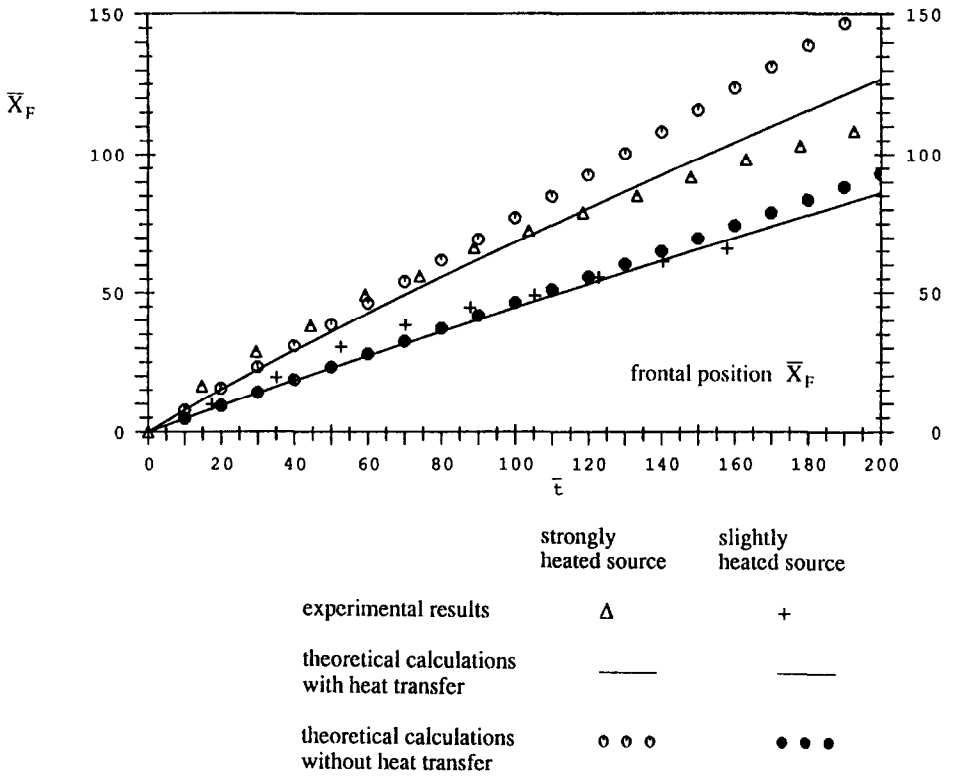

Fig. 7. Comparison of theoretical results with experiments [13] for the frontal position of a plume, from a continuous source, spreading under the ceiling.

with constant temperature only by about 10% (theoretical estimate). Measurements and theory are in reasonable agreement for this case.

The agreement is less satisfactory for the strongly heated case (Fig. 7), but several factors contribute to the discrepancies observed. The variation of some gas properties is almost negligible within the temperature range considered (the variation of c_p or Pr is smaller than 5%), but other properties, such as the thermal conductivity of the cloud or the dynamic viscosity can be reduced by about 40% during the spreading process. The plume properties are evaluated for the two extreme conditions, i.e. at the source temperature and ambient temperature. The integration, however, showed only minor discrepancies for the quantities of interest, such as velocity of the front or the temperature of the plume. The experimental temperature profiles over the height of the layer, as recorded by Chobotov, deviate considerably from the assumed tophat profiles. The box model used for the theoretical estimates, assumes that temperature, concentration, etc. over the length of the plume, vary only with time. This gives reasonable results for a fixed-volume release, but not for a continuous source. The source temperature and concentration remain constant whereas the conditions at the front change with time. This produces a spatial variation, not accounted for in the box

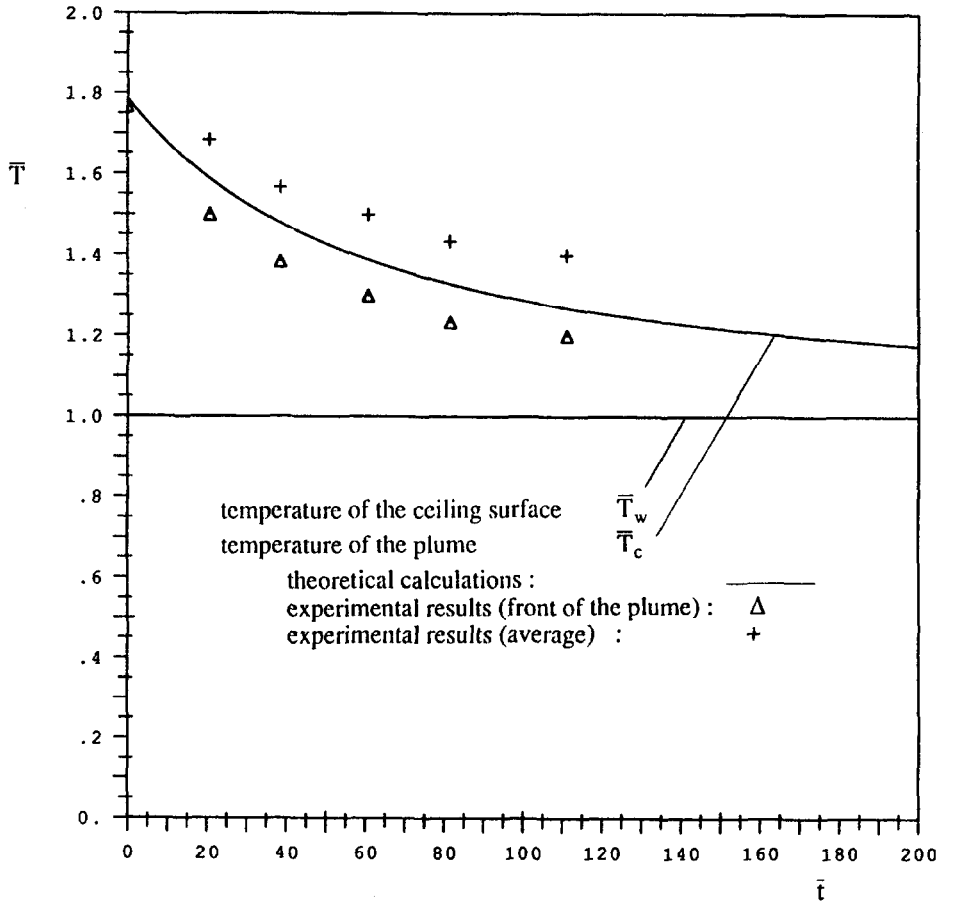

Fig. 8. Comparison of theoretical results with experiments [13] for the temperature of a plume, from a continuous source, spreading under the ceiling.

model, and it is another reason why differences between box model results and measurements are to be expected. The calculated time history of the temperature of the strongly heated plume is compared in Fig. 8 with the experimental data (where available) as recorded by Chobotov et al. The theoretical values, located between the experimental values at the front and the average values, show that the model also predicts the temperature change satisfactorily.

5. Conclusions

Experimental investigations of the spreading of dense cold clouds on warmer surfaces, or of hot fire plumes under ceilings, show strong influences of heat-transfer effects, not accounted for in conventional prediction methods.

A new model is proposed herein, which takes into account the transient heat transfer from the surface, on which the cloud spreads, as its temperature changes due to the sudden contact with the cloud or plume.

The model has been verified by comparison with experiments in 2-D channels, and satisfactory agreement is obtained both for a cold cloud spreading on a well insulated surface, and for a hot plume in contact with a good conductor.

For surfaces of practical interest, the calculations show that a dense cloud, from a cryogenic source, can be arrested by heat-transfer effects, in the absence of wind, as the negative buoyancy vanishes. The predicted hazardous range is reduced considerably, in comparison with results from conventional theoretical methods.

Nomenclature

a	thermal diffusivity
b	heat penetration coefficient
B	width of the channel
Bi	Biot number
c	concentration (mass)
c_p, c_{pa}, c_{ps}	specific heat capacity of gas (mixture, ambient, source)
C	wave velocity ($C_F = \sqrt{[(\rho - \rho_a)/\rho]gh}$)
Fo	Fourier number
Fr	densimetric Froude number
g	acceleration due to gravity
h	height of the cloud
k	empirical constant in the frontal condition
L	length (L_{ref}: reference length)
m, m_a, m_s	total mass of the cloud, mass of air, mass of gas in the cloud
$\dot{m}_a$, $\dot{m}_s$	mass-flow rate of entrained air, of the source
Nu	Nusselt number
Pr	Prandtl number
$\dot{q}$	heat flux from the ground surface
$\dot{q}_e$	heat flux related to entrainment
q_s	volume flow rate of the source (continuous release: $Q_s = q_s t$)
Q_s	volume of gas in the cloud (per unit width)
$\dot{Q}_s$	volume flow rate of the source (per unit width)
Ra	Rayleigh number
Ri	Richardson number
R, R_a, R_s	gas constant of the cloud, the ambient air and the source
St	Stanton number
t	time
t_o	time shift
T	temperature in the ground surface or in the ceiling
T_w	temperature of the surface of contact

T_c, T_a, T_s	temperature of the cloud, the ambient air and the source
U	velocity
v_e	entrainment velocity
V_s	volume of gas in the cloud
$\dot{V}_s$	volume flow rate of the source
X_F, U_F	location and velocity of the front
y	coordinate normal to the ground surface
α	heat-transfer coefficient
β	volume coefficient of expansion
δ	penetration depth of a temperature perturbation
λ_w	thermal conductivity of the surface on which the cloud spreads
λ	thermal conductivity of the cloud
ν	kinematic viscosity
ρ, ρ_a, ρ_s	density of the cloud, the ambient air and the source
Ω	$\frac{1}{3}Bi\,\bar{\delta}(\bar{t})$ (time parameter)

Subscripts/superscripts

$(\ )_a$	ambient
$(\ )_c$	cloud
$(\ )_F$	front property
$(\ )_o$	first approximation (e.g. position of the front X_{Fo})
$(\ )_s$	source
$(\ )_{ref}$	reference quantity
$(\ )_w$	property of the surface on which the cloud spreads
$(\bar{\ })$	dimensionless quantity
$\bar{t}'$	$\bar{t}' = \bar{t} + \bar{t}_0$ with time shift $\bar{t}_0$

Acknowledgements

The authors acknowledge the valuable comments and advice of Dr. D.M. Webber of AEA Technology, UK.

References

[1] J.A. Fay, Combust. Sci. Technol., 7 (1973) 47–49.
[2] P.K. Raj, J. Hazard. Mater., 5 (1981) 111–130.
[3] G.W. Colenbrander and J.S. Puttock, in: G. Ooms and H. Tennekes (Eds.), Proc. IUTAM Symp., Delft, Springer, Berlin, 1984.
[4] F. Zumsteg and T.K. Fanneløp, in: E.J. List (Ed.), Proc. 3rd Int. Symp. on Stratified Flows, 1987, ASCE, New York, 1990.
[5] R.K. Poag, Dissertation, University of Arkansas, 1987.
[6] M. Ruff, F. Zumsteg and T.K. Fanneløp, J. Hazard. Mater., 19 (1988) 51–68.

[7] R.E. Britter, Report CUED/A-Aero/TR 14 (1987), Engineering Department, Cambridge University.
[8] N.O. Jensen, J. Hazard. Mater., 3 (1983) 157–163.
[9] D.M. Webber and P.W.M. Brighton, in: S. Hartwig (Ed.), Heavy Gas and Risk Assessment, Reidel, 1986.
[10] F. Zumsteg, Ph.D. Thesis, No. 8644, Swiss Fed. Inst. of Tech., 1988.
[11] K. Emblem, P.A. Krogstad and T.K. Fanneløp, in: Proc. IUTAM Symp., Delft, 1983.
[12] A. Kneebone and L.R. Prew, Preprints. 4th LNG Conf., Algiers, 1974.
[13] M. Chobotov, E.E. Zukoski and T. Kubota, in: E.J. List (Ed.), Proc. 3rd Int. Symp. on Stratified Flows, 1987, ASCE, New York, 1990.
[14] D.E. Neff, R.N. Meroney and J.L. Cermak, CER 76–77 DEN-RNM-JSC 22. (1976), Colorado State University.
[15] J.P. Kunsch, H.P. Gröbelbauer, L. Billeter and T.K. Fanneløp, in: S. Hartwig (Ed.) Schwergasforschung an der ETH-Zürich IV. Proc. Symp. "Schwere Gase und Sicherheitsanalyse", Bonn, 26–27 September 1991.
[16] Y. Riou, Bulletin de la Direction des Etudes et Recherches, Ser. A, No 1 (1989), EDF-Electricité de France.
[17] T.K. Fanneløp, Fluid Mechanics for Industrial Safety and Environmental Protection, Industrial Safety Series, Vol. 3, Elsevier, Amsterdam, 1994.
[18] J.P. Kunsch, Numerische Berechnung der Schwergasausbreitung mit Wärmeübergang mittels Shallow-Layer Gleichungen, Interner Bericht, IFD, ETH-Zürich (1991).
[19] H.P. Gröbelbauer, T.K. Fanneløp and R.E. Britter, J. Fluid Mech., 250 (1993) 669–687.
[20] H. Gröber, S. Erk and U. Grigull, Die Grundgesetze der Wärmeübertragung, Springer, Berlin, 3rd edn., 1981.
[21] L. Prandtl, K. Oswatitsch and K. Wieghardt, Führer durch die Strömungslehre, Vieweg, 8. Auflage, 1984.
[22] J.P. Holman, Heat Transfer, McGraw-Hill, New York, 4th edn., 1976.